IEEE Access
Multidisciplinary | Rapid Review | Open Access Journal

Received December 11, 2019, accepted February 29, 2020, date of publication March 6, 2020, date of current version March 18, 2020.

Digital Object Identifier 10.1109/ACCESS.2020.2979018

Infrared Handprint Image Restoration Algorithm Based on Apoptotic Mechanism

XIAO YU, XI YE, AND QIANG GAO

School of Electrical and Electronic Engineering, Tianjin Key Laboratory for Control Theory and Applications in Complicated Systems, Tianjin University of Technology, Tianjin 300384, China

Corresponding author: Xiao Yu (yx_tjut@163.com)

This work was supported in part by the National Natural Science Foundation of China under Grant 61502340, in part by the Tianjin Natural Science Foundation under Grant 18JCQNJC01000, in part by the Scientific Research Project of Tianjin Education Commission under Grant 2018KJ133, in part by Open Funds of the Tianjin Key Laboratory for Control Theory and Applications in Complicated Systems under Grant TJKL-CTACS-201907, and in part by the National Natural Science Foundation of China under Grant 61771230.

ABSTRACT In criminal cases, the information collection and analysis of the scene plays an important role in solving cases. Handprint mark can be easily remaining and frequently occurring mark of criminals. It may occasionally be recognized as potential physical evidence during criminal investigations. The infrared thermal imager can fully collect the thermal radiation information of objects, so it is convenient to get the remaining heat source marks in the environment, and to obtain key information that is missing from other methods. Handprints tend to disappear over time. Like cell apoptosis is regulated by a rigorous mechanism of a series of genes, handprints also regulated by the mechanism of mark disappearance affected by surrounding pixels. In fact, we can easily get handprint images which hands left a period of time, but hope to restore the initial handprint image and obtain the characteristics of the criminal hand. Therefore, a method of infrared handprint image restoration based on apoptotic mechanism is proposed. Training depends on the existing infrared handprint images, and we can find a relational model between the former and the latter images. Finally, the rough shape of the original infrared handprint can be deduced.

INDEX TERMS Apoptosis mechanism, infrared handprint mark, image target restoration.

I. INTRODUCTION

In criminal cases, scene remnants often provide critical information for the detection. Studying mark image is important. In the confidential room where secret technical enterprise data are stored, through the infrared handprint image, we can judge whether the paper is touched or whether someone enters the room. In actual criminal investigations, the police cannot always arrive at the scene in the first time, and we often cannot get the remaining handprint image at different moments after the target is touched. We can get the handprint image after a period of time, such as the image of three minutes. However, we hope that, through some means, the initial handprints can be restored and the hand characteristics of the criminals can be judged, such as the length of the fingers and the outline of the hands. It is necessary to propose a method to restore infrared handprint mark image for solving practical problems.

The associate editor coordinating the review of this manuscript and approving it for publication was Sunil Karamchandani.

Infrared image technology is a non-contact detection technology which converts invisible thermal radiation into visible thermal image [1]. Under the analysis of infrared images, many scholars run continuous researches, and have made many achievements. In 2013, Chen C. L. P. *et al.* present an effective small target detection algorithm inspired by the contrast mechanism of human vision system and derived kernel model [2]. In 2015, Pucci .M *et al.* apply an active infrared thermography to study a seventeenth-century painting on paper [3]. And thermography is performed before and after restoration to obtain information used in planning the restoration and also to assess its effectiveness. In 2016, Chen Shuyue *et al.* introduce a method based on Gauss point spread function to enhance the clarity and contrast of the heat source [4]. In 2018, Zhang Su *et al.* propose a method for detecting dim and small targets in infrared images based on temporal and spatial non-local similarity, which utilizes the non-local autocorrelation between infrared image sequences of adjacent frames and the similarity between non-local background image blocks in each frame [5]. In 2018, Xu Ming *et al.* propose a full convolution network pedestrian

detection algorithm based on saliency detection in frequency domain for thermal infrared surveillance scene, which realizes end-to-end training of detection algorithm and improves the performance of pedestrian detection in thermal infrared surveillance system [6].

Infrared equipment, applied to criminal cases, is used more and more widely. Many researches are based on infrared spectrum. The work in [7] investigates a handheld near-infrared spectrometer for the specific identification of deposited bloodstains. The work in [8] describes an innovative modeling method for discriminating the ATR FT-IR spectra of various body fluids, including peripheral blood, saliva, semen, urine and sweat, to meet the practical demands in criminal investigations. The work in [9] aimed at multilayered automotive paint fragments, which provide crucial links in criminal investigations and prosecutions. To determine the origin of these paint fragments, its improved method permits intercomparison of OEM automotive paint layer systems using the IR spectra alone. But these researches are almost about chemistry method, they are not very intuitive. The testing instruments are precise and complex; we cannot get results at the scene immediately. Through infrared thermal imager, the traces can be obtained quickly and easily, which improves efficiency.

Biologically, to maintain the stability of the number of cells in the organism itself, programmed cell death, or apoptosis, occurs, which is strictly regulated by a series of genes. This regulation relationship can be applied to our construction of infrared handprint image restoration model. The disappearance of mark is affected and controlled by the surrounding pixels.

In recent years, many scholars at home and abroad have been deepening the study of apoptotic mechanism. In 2010, Shi Yigong *et al.* summarize recent advances in structural biology in the regulation of apoptotic molecules, mainly Caspase and protein functions directly related to Caspase activity regulation [10]. In 2014, Chai Jijie and Shi Yigong review recent advances in the activation mechanism of apoptotic and inflammatory complexes [11]. In 2017, Candeias E *et al.* find that GLP-1/IGF-1 signaling and autophagy mediate Exendin-4have protective effects on apoptosis in type 2 diabetic rats [12]. And a promising treatment against the chronic complications of Type 2 diabetes affecting the brain is discussed. In 2018, Zhou H *et al.* confirm that CK2 alpha serves as a negative regulator of mitochondrial homeostasis via suppression of FUNDC1-required mitophagy, favoring the development of cardiac IR injury [13]. In 2018, Galluzzi Lorenzo *et al.* unveil novel mechanisms that orchestrate multiple cell death pathways, and propose an updated classification of cell death subroutines focusing on mechanistic and essential aspects of the process [14].

Based on the mechanism of cell apoptosis and considering the correlation of time series, we propose an infrared handprint image restoration algorithm. Firstly, the training process is used to construct a gray-scale feature model of the infrared handprint image from the previous moment to the next moment. Six feature points are collected from the previous moment infrared handprint image, and their gray values are obtained; then six points in the same positions are found in the next moment infrared handprint mark image, and the gray values of the pixels and their four neighborhoods are obtained; using the four-neighborhood gray values and the gray values of the feature points at the previous moment image, the functional relation is constructed and the relational coefficient is calculated; the best segmentation threshold of the previous moment infrared handprint is obtained by maximum inter-class variance, and the range of function model is determined by adjusting parameters; several sets of infrared handprint image models based on time series transformation are constructed continuously and their scope of action is determined. The model obtained from the training process can eventually deduce the rough shape of the original infrared handprint image from the last minute infrared handprint image.

II. PROBLEM ANALYSIS

Under the law of thermodynamics, the system we study is always in the process of change and development. It acts with the environment through the border and exchanges energy, such as work and heat. There are many spontaneous processes in nature, for instance, the spontaneous transfer of heat from a high-temperature object to a low-temperature object, which is caused by potential difference [15].

In the experiment, people put their hands on the wall and left some marks of temperature. Because the hand temperature is slightly higher than the wall temperature, there is a temperature difference between the system and the environment. The temperature difference is the driving force of heat transfer, and there is heat transfer with temperature difference. The heat transfer process can be divided into three modes: heat conduction, thermal radiation and thermal convection.

Actually, the thermal transmission is often superimposed by a variety of heat transfer modes, involving many factors such as wind speed, light, temperature and so on.

A. THE CASE ANALYSIS

A real case occurred in a village in Tancheng, Linyi City, Shandong Province, China. It was a hazy sunrise in July. A middle-aged man who lived opposite his mother's house heard some weird noise outside. Through the windows, he saw his mother and the psychopath who lived next to her pushing her room's door back and forth. His mother bowed her head and pushed hard at the door in a half kneeling position. The man ran to his mother at once but it was still late. The psychopath has left and the old lady was dead. The old lady felled to her knees. Her head was bloodstained. And the outside door handle was missing.

No evidence was found at the scene. The psychopath was most likely a suspect. The head of the victim was obviously injured by sharp objects. Later, the police found the missing door handle in the house of the psychopath. There is no

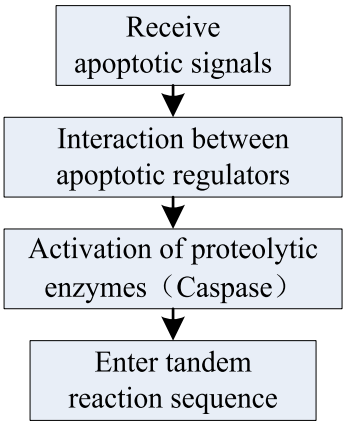

FIGURE 1. Apoptotic process.

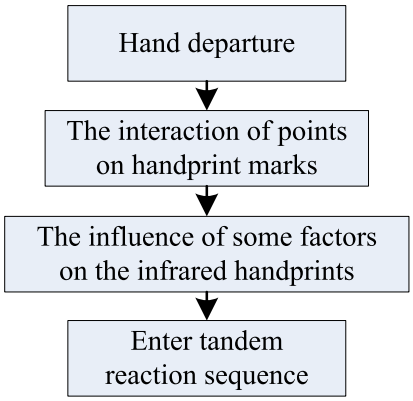

FIGURE 2. 'Apoptotic' process of handprint image.

suspect's or victim's DNA on it after laboratory tested. The investigation of the case has fallen into a bottleneck.

After a long time of investigation, the investigators finally found that there was a nail in the inner bolt. The nail was stained with the victim's bloodstain. In the process of two people pushing the door back and forth, the nail cut through the fragile part of the old lady's head and caused her death.

In this case, if we have a chance to use an infrared thermal imager for investigation, we can quickly find unusual traces about the nail or anything else. In larceny cases, although suspects wear gloves or wipe marks, the heat traces will not disappear in a period of time. Through the rapid and comprehensive inspection of the scene by the infrared thermal imager, the efficiency of solving cases is increased. Also, save time, manpower and material resources.

B. APOPTOTIC MECHANISM

In general organisms, the number of cells needs to be precisely regulated. Apoptosis refers to the spontaneous and orderly death of cells controlled by genes, also known as programmed cell death, in order to maintain the stability of the organismic internal environment [16], [17]. Apoptosis is an active process involving the activation, expression and regulation of a series of genes. Normal regulation of apoptosis is closely related to cancer, autoimmune diseases, neurodegenerative diseases and other diseases. If cells proliferate too much, they cause cancer. If there are too many apoptotic cells, neurodegenerative diseases such as Alzheimer's disease can be caused. Apoptosis regulation must be controlled strictly. The general process of apoptosis is shown in Figure. 1.

C. CHARACTERISTIC ANALYSIS OF INFRARED HANDPRINT IMAGE

Each pixel on the infrared handprint image is regarded as a cell in the organism. As time goes by, the infrared handprint mark will gradually disappear, which can be seen as the apoptosis of cells. Cell apoptosis is strictly regulated by a series of genes, and the disappearance of infrared handprint mark is also affected by a series of factor6s, such as the four neighborhoods of a pixel. The process of approximate 'Apoptosis' of infrared handprint image is shown in Figure. 2. The infrared handprint scene is shown in Figure. 3.

Under visible light conditions, it is hard to judge whether the wall has been touched or not. But through infrared spectroscopy images, it is much easier. In actual investigation scene, images we collected are always several minutes later. In this paper, for instance, ideally, we discuss about 3-minute images. When the hand has left the wall for about 3 minutes, although there are still some handprints, no specific marks of the hand can be distinguished. We simplify complex nonlinear problems. Build three models to establish the relation between 1-second and 1-minute infrared handprint images, 1-minute and 2-minute infrared handprint images, 2-minute and 3-minute infrared handprint images. Each relation is affected by different factors. Thus, the initial appearance of the handprint is restored by the 3-minute (last) infrared handprint image. If the process is simplified, the error of recovery will appear. The effect of restoring handprint is not very good. We need smaller time intervals, but this increases the complexity of the calculation.

III. INFRARED HANDPRINT MARK IMAGE RESTORATION ALGORITHM BASED ON APOPTOSIS

A. APOPTOTIC PROCESS

The gene regulation mechanism of apoptosis was firstly made from the study of *Caenorhabditis elegans*. The four genes of EGL-1, CED-9, CED-4 and CED-3 strictly controlled the programmed death of nematode cells. CED-3 encodes a cysteine protease CED-3, which is activated by CED-4. The function of CED-4 is inhibited by CED-9, and CED-9 is inhibited by EGL-1. They form a precise regulatory system. In mammalian cells, the process of apoptosis is usually divided into exogenous and endogenous pathways. Caspase family is closely related to the regulation of apoptosis [10], [18]. The approximate apoptotic process is shown in Figure. 4.

In the exogenous pathway, the external inducer of the cell triggers the 'death receptor', sends out a death signal, activates Caspase-8, and thus performs apoptosis. In the

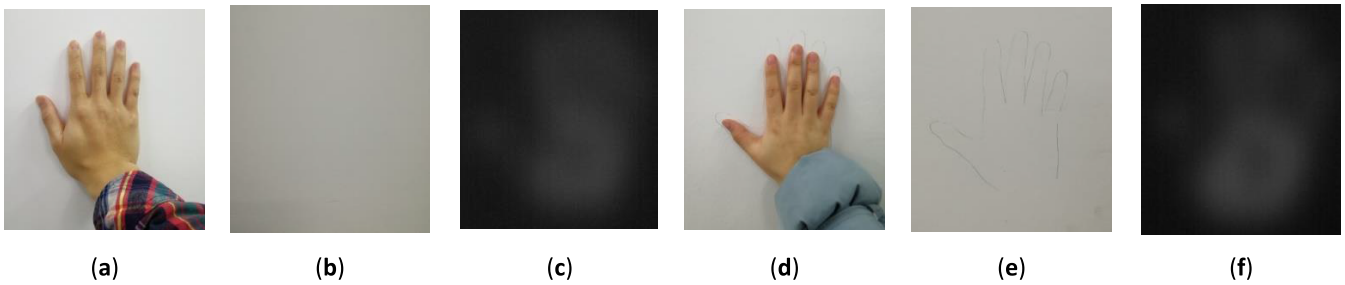

FIGURE 3. Infrared handprint scene(the temperature is about 19°C to 24°C, humidity is about 40% to 50%, indoor, no wind, daytime; and the testing hands are in good conditions): (a) Hand original image I; (b) Wall visible light image I; (c) Leave 3 minutes mark I; (d) Hand original image II; (e) Wall visible light image II; (f) Leave 3 minutes mark II.

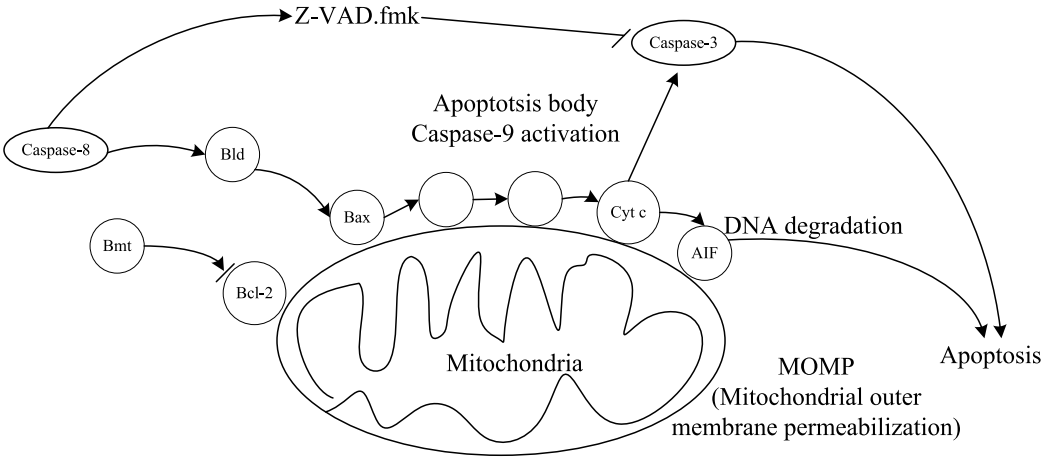

FIGURE 4. Apoptosis (AIF: Apoptosis inducing factor; Cyt-c: Cytochrome c; Z-VAD.fmk: Valine-alanine-aspartate).

endogenous pathway, cell apoptosis is triggered by intracellular events (such as DNA damage). Cytochrome c is released by Bcl family proteins on the outer membrane of mitochondria. Cytochrome c interacts with a large protein, Apaf-1, to activate the initial Caspase-9, and then downstream effects such as Caspase-3 and-7 are activated. In mammalian cells, there are factors that regulate this process, namely apoptosis inhibitory proteins (IAPs). IAPs can bind to Caspase-9 and Caspase-3, -7, preventing their enzyme activity.

B. CONSTRUCTION OF INFRARED HANDPRINT MARK RESTORATION MODEL

The disappearance process of handprint image can be analogized to the process of apoptosis. According to the laws of thermodynamics, the disappearance of handprints is superimposed by a variety of heat transfer modes. Heat conduction usually occurs inside the object, similar to the endogenous pathway of apoptosis. Thermal convection and thermal radiation occur at the boundary of the object and can be similar to the exogenous pathway of apoptosis.

Due to the diversity of the environment and the different heat dissipation of different material carriers, the handprint image cannot be completely preserved. It is necessary to construct a model to restore the approximate appearance of the handprint image to get more information. Figure. 5 is a flow chart of the infrared handprint mark restoration algorithm.

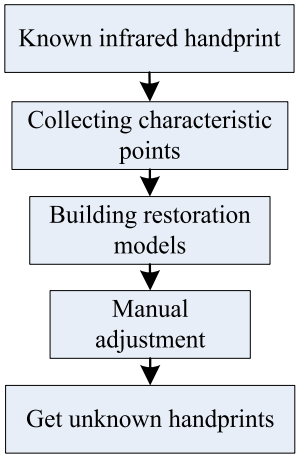

FIGURE 5. Infrared handprint image restoration algorithm flow chart.

In order to construct restoration models of infrared handprint marks, it is necessary to carry out a training process firstly to find the relationship between the remaining handprint mark images as time passes. Using infrared cameras, the handprint images on the wall are collected, which

are after the hand left for 1 second, 1 minute, 2 minutes and 3 minutes. The reason why we chose this three kind of handprint images is that we want to simplify the complex problem. If the time interval is very small (approach zero), we can regard nonlinear problems as linear problems approximately.

If the gray value relation between 1-second and 1-minute infrared handprint mark images is found, then the relational model between the two images is constructed, thus we can complete the process of inferring one second infrared handprint mark from 1-minute infrared handprint mark. Based on the previous experience, six feature points are selected from the center of palm and each finger. Manual selection can be quickly and accurately. These six areas respectively represent the thumb, index finger, middle finger, ring finger, little thumb and palm part of the hand. The correlation between them is low, and the feature difference is obvious. Firstly, six pixels $x_{00}, x_{01}, x_{02}, x_{03}, x_{04}$ and x_{05} are selected in the known one-second hand-print gray-scale image, and the gray-scale values of the six pixels are obtained as follows:

$$\begin{aligned} &x_{00} = I_0(i_0, j_0); \quad x_{01} = I_0(i_1, j_1); \quad x_{02} = I_0(i_2, j_2); \\ &x_{03} = I_0(i_3, j_3); \quad x_{04} = I_0(i_4, j_4); \quad x_{05} = I_0(i_5, j_5) \end{aligned} \tag{1}$$

The size of one second hand-print gray-scale image I_0 is $M \times N$, i and j are coordinate positions in the image. $i = 0, 1, \ldots, M, j = 0, 1, \ldots, N$. Generally, the pixel points we select are the points in the figure that can reflect more gray information, that is, the local central area or the area with large gray value.

In the infrared handprint mark image I_1, after the hand left 1 minute, six pixel points x_{10}, x_{11}, x_{12}, x_{13}, x_{14}, x_{15} which are the same positions as those selected in the one-second handprint mark image are found. The gray value and the gray value of its four neighborhood points respectively are

$$\begin{aligned} &x_{10} = I_1(i_0, j_0); \quad x_{11} = I_1(i_1, j_1); \quad x_{12} = I_1(i_2, j_2); \\ &x_{13} = I_1(i_3, j_3); \quad x_{14} = I_1(i_4, j_4); \quad x_{15} = I_1(i_5, j_5) \\ &I_1(i_0, j_0 - 1), \quad I_1(i_0, j_0 + 1), \; I_1(i_0 - 1, j_0), \; I_1(i_0 + 1, j_0); \\ &I_1(i_1, j_1 - 1), \quad I_1(i_1, j_1 + 1), \; I_1(i_1 - 1, j_1), \; I_1(i_1 + 1, j_1); \\ &I_1(i_2, j_2 - 1), \quad I_1(i_2, j_2 + 1), \; I_1(i_2 - 1, j_2), \; I_1(i_2 + 1, j_2); \\ &I_1(i_3, j_3 - 1), \quad I_1(i_3, j_3 + 1), \; I_1(i_3 - 1, j_3), \; I_1(i_3 + 1, j_3); \\ &I_1(i_4, j_4 - 1), \quad I_1(i_4, j_4 + 1), \; I_1(i_4 - 1, j_4), \; I_1(i_4 + 1, j_4); \\ &I_1(i_5, j_5 - 1), \quad I_1(i_5, j_5 + 1), \; I_1(i_5 - 1, j_5), \; I_1(i_5 + 1, j_5) \end{aligned} \tag{2}$$

Construct a 1-minute handprint mark image in the pixel four neighborhood gray value as a function of the corresponding pixel point gray value in the one second handprint mark image, with four coefficients *a, b, c, d*(both constant), to establish a simple function equation, as follows:

$$\begin{cases} I_0(i_0, j_0) = aI_1(i_0, j_0 - 1) + bI_1(i_0, j_0 + 1) + cI_1(i_0 - 1, j_0) \\ \qquad + dI_1(i_0 + 1, j_0) \\ I_0(i_1, j_1) = aI_1(i_1, j_1 - 1) + bI_1(i_1, j_1 + 1) + cI_1(i_1 - 1, j_1) \\ \qquad + dI_1(i_1 + 1, j_1) \\ I_0(i_2, j_2) = aI_1(i_2, j_2 - 1) + bI_1(i_2, j_2 + 1) + cI_1(i_2 - 1, j_2) \\ \qquad + dI_1(i_2 + 1, j_2) \\ I_0(i_3, j_3) = aI_1(i_3, j_3 - 1) + bI_1(i_3, j_3 + 1) + cI_1(i_3 - 1, j_3) \\ \qquad + dI_1(i_3 + 1, j_3) \\ I_0(i_4, j_4) = aI_1(i_4, j_4 - 1) + bI_1(i_4, j_4 + 1) + cI_1(i_4 - 1, j_4) \\ \qquad + dI_1(i_4 + |1, j_4) \\ I_0(i_5, j_5) = aI_1(i_5, j_5 - 1) + bI_1(i_5, j_5 + 1) + cI_1(i_5 - 1, j_5) \\ \qquad + dI_1(i_5 + 1, j_5) \end{cases} \tag{4}$$

The four coefficients correspond to the characteristics of each part of the four fields. The reason why we set the coefficients as constant is to simplify the calculation. Although the operation increases the error to some extent, it is still within the acceptable range. By solving this equation, the gray value relational coefficients a, b, c, and d of each pixel in 1-minute and 1-second handprint marks can be obtained. Using the four relational coefficients obtained by equation (4), the partial pixel points are counteracted in the 1-minute handprint mark image, so that the approximate appearance of the one second handprint mark image can be inferred.

Similarly, a group of 1-minute and 2-minute hand-print images, and a group of 2-minute and 3-minute hand-print images can be used to find the approximate relational model between the gray values of the pixels in the two images. In this training process, the known are the input gray image (infrared handprint image at the previous moment) and the output gray image (infrared handprint image at the latter moment). What we need to find is the systematic relation between the two.

C. DETERMINING THE SCOPE OF THE IMAGE RESTORATION MODEL

Based on a specific experimental environment, we can know the fact that the environment (include temperature, humidity, wind speed and so on) is relatively stable. The background area of the handprint image obtained by the infrared camera does not change much. When using the coefficient relation to reverse the infrared handprint mark image of the previous moment, the relation should be applied to the target area (hand area) in the image instead of the entire image. During the training process, the Otsu threshold segmentation algorithm [19], [20] can be used to segment the infrared handprint image of the previous moment (e.g. one second) to obtain the optimal segmentation threshold t^*.

For a specific infrared handprint image, a threshold range is obtained by adjusting t^* up and down. The pixels in this range are transformed by the relational coefficients. And the

TABLE 1. Coordinates and gray values of six pixels in the one second image.

Coordinate position	Grey scale
(126,37)	206
(41,93)	207
(35,137)	199
(48,165)	195
(84,195)	189
(184,90)	233

TABLE 2. Gray values of six pixels and their four neighborhoods in 1-minute image.

Coordinate position	Grey scale	Gray values of points in four neighborhoods			
(126,37)	57	58	58	57	56
(41,93)	65	65	64	63	66
(35,137)	67	67	68	68	66
(48,165)	58	61	58	60	58
(84,195)	60	59	56	60	58
(184,90)	103	103	103	104	101

handprint image of the previous moment can be derived from the latter moment image.

IV. RESULTS AND ANALYSIS

The indoor environment temperature is around 19°C to 24°C, humidity is about 40% to 50%, no wind. Several sets of infrared handprint mark on the wall were taken by the infrared camera Fluke Tix640.

A. CONSTRUCTING GRAY-SCALE MODEL OF INFRARED HANDPRINT AND SEARCHING SCOPE

1) ONE SECOND AND 1-MINUTE INFRARED HANDPRINT IMAGES

Search six pixel points in the one-second infrared handprint mark image, and record its coordinate position and gray value, as shown in Table 1. In the 1-minute image, six pixels with the same coordinates are found, and the gray value and the gray value of the four neighborhoods are recorded, as shown in Table 2. The optimal segmentation threshold t^* of target and background in the one second image is 110.007 by using the method of maximum inter-class variance.

The relational model between two infrared handprints is constructed, and the coefficients are 24.3802, −5.5444, −13.8414 and −2.2426. Then the relation between one second and 1-minute infrared handprints is as follows.

$$I_{1s}(i,j) = 24.3802^* I_{1\,\min}(i,j-1) - 5.5444^* I_{1\,\min}(i,j+1) - 13.8414^* I_{1\,\min}(i-1,j) - 2.2426^* I_{1\,\min}(i+1,j) \quad (5)$$

2) 1-MINUTE AND 2-MINUTE INFRARED HANDPRINT IMAGES

Search six pixel points in the 1-minute infrared handprint mark image, and record its coordinate position and gray value, as shown in Table 3. In the 2-minute image, six pixels with the same coordinates are found, and the gray value and the gray value of the four neighborhoods are recorded, as shown in Table 4. The optimal segmentation threshold t^* of target and background in the 1-minute image is 49.011 by using the method of maximum inter-class variance.

TABLE 3. Coordinates and gray values of six pixels in the 1-minute image.

Coordinate position	Grey scale
(126,37)	57
(41,93)	65
(35,137)	67
(48,165)	58
(84,195)	60
(184,90)	103

TABLE 4. Gray values of six pixels and their four neighborhoods in the 2-minute image.

Coordinate position	Grey scale	Gray values of points in four neighborhoods			
(126,37)	36	36	36	36	36
(41,93)	42	42	44	44	43
(35,137)	49	50	48	49	48
(48,165)	41	43	40	41	40
(84,195)	38	39	38	37	38
(184,90)	70	73	70	70	70

TABLE 5. Coordinates and gray values of six pixels in the 2-minute image.

Coordinate position	Grey scale
(126,37)	36
(41,93)	42
(35,137)	49
(48,165)	41
(84,195)	38
(184,90)	70

TABLE 6. Gray values of six pixels and their four neighborhoods in the 3-minute image.

Coordinate position	Grey scale	Gray values of points in four neighborhoods			
(126,37)	29	32	30	29	29
(41,93)	38	37	38	38	37
(35,137)	39	39	40	40	40
(48,165)	36	37	36	36	38
(84,195)	31	31	30	33	32
(184,90)	59	60	60	58	59

The relational model between two infrared handprints is constructed, and the coefficients are −1.0320, 0.5926, −2.4844, and 4.4554. Then the relation between 1-minute and 2-minute infrared handprints is as follows.

$$I_{1\mathrm{min}}(i,j) = -1.0320^* I_{2\,\min}(i,j-1) + 0.5926^* I_{2\,\min}(i,j+1) - 2.4844^* I_{2\,\min}(i-1,j) + 4.4554^* I_{2\,\min}(i+1,j) \quad (6)$$

3) 2-MINUTE AND 3-MINUTE INFRARED HANDPRINT IMAGES

Search six pixel points in the 2-minute infrared handprint mark image, and record its coordinate position and gray

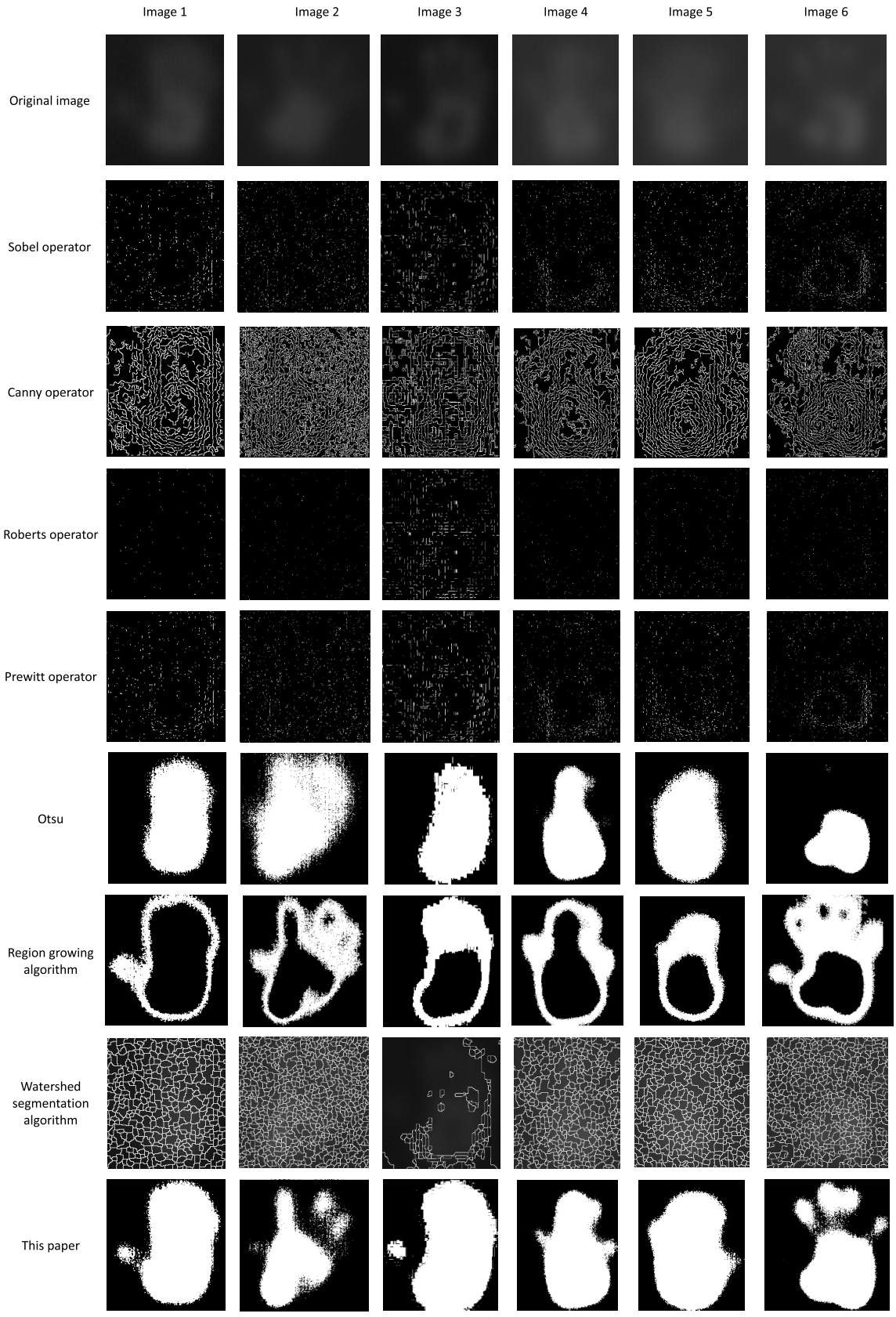

FIGURE 6. Comparison of experimental results.

value, as shown in Table 5. In the 3-minute image, six pixels with the same coordinates are found, and the gray value and the gray value of the four neighborhoods are recorded, as shown in Table 6. The optimal segmentation threshold t^* of target and background in the 2-minute image is 37.0005 by using the method of maximum inter-class variance.

The relational model between two infrared handprints is constructed, and the coefficients are 0.4305, 0.2476, 0.7542 and −0.2539. Then the relation between 2-minute and 3-minute infrared handprints is as follows.

$$I_{2\min}(i,j) = 0.4305^* I_{3\min}(i,j-1) + 0.2476^* I_{3\min}(i,j+1) + 0.7542^* I_{3\min}(i-1,j) - 0.2539^* I_{3\min}(i+1,j) \tag{7}$$

B. EXPERIMENTAL SIMULATION RESULTS AND ANALYSIS

Six 3-minute infrared handprint mark images with the same shooting conditions are processed by Sobel, Canny, Roberts, Prewitt operators, one-dimensional OTSU algorithm, region growth algorithm, watershed segmentation algorithm and our algorithm respectively. The results are shown in Figure. 6.

From the comparison of the results, it can be seen that Sobel, Canny, Roberts, Prewitt operators and watershed segmentation algorithm are difficult to draw the outline of handprint images, and the segmentation results are bad. The one-dimensional Otsu algorithm only extracts part of the target area of handprint images, and it is incomplete. The region growing algorithm is better than one-dimensional Otsu algorithm in extracting target contour, but there are large uncertain regions (black areas) in the target. The algorithm in this paper can locate and restore the outline of the handprint mark more accurately, give the positions of thumb or pinkie especially in Image 1, 3, 4 and 5.The uncertainty area is much smaller. Therefore, our algorithm is better than other traditional methods in processing infrared handprint mark images.

In order to further detect the accuracy of the algorithm, the extracted result (EI) is quantitatively evaluated, and the result is manually extracted as a reference standard image (Ground Truth, GT), that is, the evaluation basis. The schematic diagram of the relationship between the reference standard and the extraction results is shown in Figure.7. Concretely, true Positive (TP) represents the number of pixels that are correctly classified as the target. True Negative (TN) indicates the number of pixels that are correctly classified as the background. False Positive (FP) denotes the number of pixels misclassified as the target. False Negative (FN) denotes the number of pixels incorrectly classified as the background.

Firstly, a factor Y is proposed to distinguish whether the classifier is good or not, that is,

$$\mathrm{Y} = \left(\frac{\mathrm{TP}}{\mathrm{TP}+\mathrm{FN}} - 1\right)^2 + \left(\frac{\mathrm{FP}}{\mathrm{FP}+\mathrm{TN}}\right)^2 = \left(\frac{\mathrm{FN}}{\mathrm{TP}+\mathrm{FN}}\right)^2 + \left(\frac{\mathrm{FP}}{\mathrm{FP}+\mathrm{TN}}\right)^2 \tag{8}$$

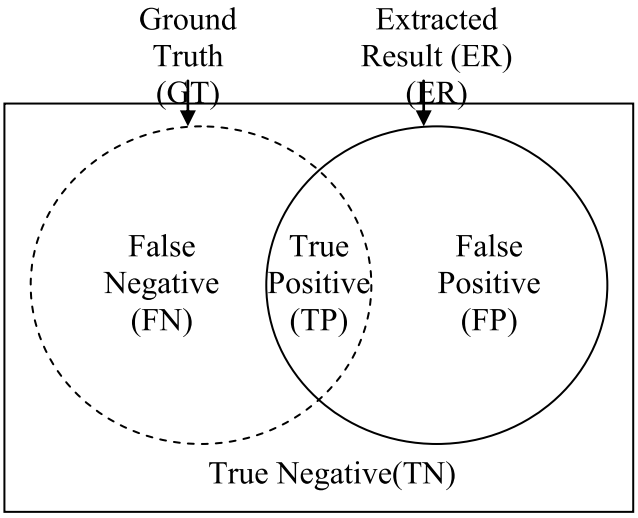

FIGURE 7. A schematic diagram of the relationship between reference criteria and extraction results.

This factor directly reflects the quality of the classifier, that is, the closer the value of Y approaches zero, the better the classifier is. Because FPR = 0, TPR = 1, that is, $\left(\frac{\mathrm{FP}}{\mathrm{FP}+\mathrm{TN}} = 0, \frac{\mathrm{TP}}{\mathrm{TP}+\mathrm{FN}} = 1\right)$, it represents the optimal classifier. The new discriminant factor Y represents the degree of difference between the discriminant classifier and the best classifier. The smaller the value of Y is, the smaller the difference between the discriminant classifier and the best classifier is. The Y value in formula (8) includes two items: one is $\left(\frac{\mathrm{TP}}{\mathrm{TP}+\mathrm{FN}} - 1\right)^2$, which represents the square of the complement set of true positive rate. And the true positive rate should be assigned as the proportion of the target actually the number of targets to the true target number. The true positive rate is the best when the true positive rate is 1, $\left(\frac{\mathrm{TP}}{\mathrm{TP}+\mathrm{FN}} - 1\right)^2$ represents the difference degree from the optimal classifier. The smaller the value is, the closer the true positive rate is to 1, and the better the classifier is. The other one is $\left(\frac{\mathrm{FP}}{\mathrm{FP}+\mathrm{TN}}\right)^2$, which indicates the square of the false positive rate. The false positive rate is the percentage that should be assigned as the background but is assigned as the target number to the real background. The smaller the value is, the smaller the misclassification rates of the background is, and the better the classifier is.

Secondly, a factor X is proposed to distinguish whether the classifier is good or not, that is,

$$\mathrm{X} = \frac{\mathrm{FN}+\mathrm{FP}}{\mathrm{FN}+\mathrm{FP}} = \frac{\mathrm{FN}+\mathrm{FP}}{\mathrm{P}} \tag{9}$$

$P = FN + TP$ represents the sum of the actual target which is misclassified into the background plus the actual target which is correctly classified as the sum of the number of targets, that is, the total number of real targets. $FN + FP$ represents the number of actual goals that are misclassified as backgrounds plus the number of actual backgrounds that are misclassified as goals. It can be said that $FN + FP$ represents

TABLE 7. Quantitative analysis of contrast experiments.

Image	Index	Sobel	Canny	Roberts	Prewitt	Otsu	Region growing	Watershed	This paper
1	Y	0.9627	0.6814	0.9953	0.9624	0.0651	0.8856	0.6799	0.0388
	X	1.0094	1.0817	1.0014	1.0102	0.4952	1.3794	1.1279	0.4005
2	Y	0.9644	0.6526	0.9954	0.9630	0.1580	0.5752	0.6805	0.1080
	X	1.0098	1.1554	1.0026	1.0096	0.8074	1.2057	1.1159	0.5000
3	Y	0.9263	0.7423	0.9379	0.9308	0.0845	0.3726	0.9025	0.1438
	X	1.0195	1.0944	1.0190	1.0187	0.6334	0.9331	1.0097	0.6719
4	Y	0.9636	0.6973	0.9937	0.9573	0.0620	0.7952	0.7050	0.0779
	X	1.0074	1.0997	1.0015	1.0076	0.4346	1.5466	1.1233	0.5369
5	Y	0.9602	0.7125	0.9919	0.9622	0.0632	0.3543	0.7021	0.1238
	X	1.0117	1.1401	1.0038	1.0094	0.5131	0.8634	1.1553	0.6781
6	Y	0.9517	0.6861	0.9911	0.9624	0.2285	0.5033	0.6951	0.0816
	X	1.0129	1.1205	1.0042	1.0091	0.5362	1.4363	1.1709	0.6333

the sum of the number of misclassified content. Definition X is the proportion of the sum of the number of misclassified content to the total number of real goals. Since the total number P of the real targets is constant, then the smaller the number of contents that are misclassified is, the smaller the value of X is, and the better the classifier effect is. Therefore, the smaller the value of the X is, the closer it is to zero, and the less the misclassified content is, the better the classifier is.

Using Y and X to discriminate the image segmentation effect jointly, we hope that the obtained values are both smaller. The results of Y and X are shown in Table 7.

It can be found from the table that the indexes of Sobel, Canny, Roberts, Prewitt operator and watershed segmentation algorithm are generally higher, which indicates that edge detection algorithm and watershed algorithm are not suitable for extracting infrared handprint images after a period of time. The indexes of the proposed algorithm are smaller than those of the region growing algorithm, so our algorithm is better. In Image 1, 2 and 6, the indexes of our algorithm is smaller than those of one-dimensional Otsu algorithm. In Image 3, 4 and 5, the indexes of one-dimensional Otsu algorithm is slightly smaller than that our algorithm, but the difference is little. From the segmentation results, one-dimensional Otsu algorithm loses part of the handprint information, while our algorithm covers more information such as the positions of thumb or pinkie. Therefore, the proposed algorithm is better than one-dimensional Otsu algorithm and other traditional segmentation algorithms in the restoration of infrared handprint mark images.

V. CONCLUSION

Aiming at the characteristics of infrared handprint mark images, this paper proposed a simple infrared handprint mark image restoration method based on the mechanism of apoptosis. The method includes a training process and an implementation process. Given infrared handprint mark images of the previous moment and the latter moment, the connection model between the two is established, and the maximum inter-class variance method is used to calculate the optimal segmentation threshold. The parameter values are adjusted. Based on the correlation of time series, models with different coefficients are constructed to realize the restoration of the approximate infrared handprint image. The results show that our algorithm is simple and feasible. It can restore the infrared handprint image from 3 minutes to 1 second. This paper only considers the influence of four neighborhood pixels. In fact, the disappearance of infrared handprint mark images is also affected by many factors such as environment, hand temperature, contact material, etc., and needs specific analysis.

ACKNOWLEDGMENT

The authors would like to thank anonymous reviewers for providing constructive suggestions that aided in improvisation of this manuscript.

REFERENCES

[1] C. J. Rong, X. G. Cao, and X. Z. Bai, "Infrared Dim and Small Target Detection Algorithm Combining Directional Derivative Feature of Facet With Sparse Representation," *Chin. J. Image Graph.*, vol. 23, no. 11, pp. 156–164, 2018. [Online]. Available: http://www.cjig.cn/jig/ch/reader/view_abstract.aspx?doi=10.11834/jig.180258, doi: 10.11834/jig.180258.

[2] C. L. Philip Chen, H. Li, Y. Wei, T. Xia, and Y. Yan Tang, "A local contrast method for small infrared target detection," *IEEE Trans. Geosci. Remote Sens.*, vol. 52, no. 1, pp. 574–581, Jan. 2014, doi: 10.1109/TGRS.2013.2242477.

[3] M. Pucci, C. Cicero, N. Orazi, F. Mercuri, U. Zammit, S. Paoloni, and M. Marinelli, "Active infrared thermography applied to the study of a painting on paper representing theChigi's family tree," *Stud. Conservation*, vol. 60, no. 2, pp. 88–96, Mar. 2015, doi: 10.1179/2047058413Y.0000000117.

[4] S. Y. Chen, S. S. Zhu, and X. Jiang, "Heat source restoration of infrared images based on Gaussian point spread function," *Laser Technol.*, vol. 40, no. 2, pp. 270–273, 2016. [Online]. Available: http://www.jgjs.net.cn/cn/article/doi/10.7510/jgjs.issn.1001-3806.2016.02.025, doi: 10.7510/jgjs.issn.1001-3806.2016.02.025.

[5] S. Zhang, B. W. An, and S. D. Pan, "Infrared dim target detection based on temporal-spatial non-local similarity," *Acta Photonica Sinica*, vol. 47, no. 11, pp. 253–263, Nov. 2018, doi: 10.3788/gzxb20184711.1110001.

[6] M. Xu, X. S. Yu, and D. Y. Chen, "Pedestrian detection in complex thermal infrared surveillance scene," *J. Image Graph.*, vol. 23, no. 12, pp. 1829–1837, 2018, doi: 10.11834/jig.180299.

[7] A. V. Morillas, J. Gooch, and N. Frascione, "Feasibility of a handheld near infrared device for the qualitative analysis of bloodstains," *Talanta*, vol. 184, pp. 1–6, Jul. 2018, doi: 10.1016/j.talanta.2018.02.110.

[8] T. Ayari, "Soft and robust identification of body fluid using Fourier transform infrared spectroscopy and chemometric strategies for forensic analysis," *Sci. Rep.*, vol. 8, no. 1, pp. 1–10, May 2018.

[9] B. K. Lavine, C. G. White, M. D. Allen, and A. Weakley, "Pattern recognition-assisted infrared library searching of the paint data query database to enhance lead information from automotive paint trace evidence," *Appl. Spectrosc.*, vol. 71, no. 3, pp. 480–495, Mar. 2017, doi: 10.1177/0003702816666287.

[10] Y. G. Shi and B. F. Sun, "Mechanisms of programmed cell death through structural biology," *Chin. Bull. Life Sci.*, vol. 22, no. 3, pp. 224–228 2010, doi: 10.13376/j.cbls/2010.03.004.

[11] J. J. Chai and Y. G. Shi, "Apoptosome and inflammasome: A caspase-activating platform," *Progr. Biochem. Biophys.*, vol. 41, no. 10, pp. 1056–1062, 2014. [Online]. Available: http://www.pibb.ac.cn/pibbcn/ch/reader/view_abstract.aspx?file_no=20140285&flag=1, doi: 10.3724/SP.J.1206.2014.00285.

[12] E. Candeias, S. In Sebastiao, and S. Cardoso, "Brain GLP-1/IGF-1 signaling and autophagy mediate exendin-4 protection against apoptosis in type 2 diabetic rats," *Mol. Neurobiol.*, vol. 55, pp. 4030–4050, May 2018, doi: 10.1007/s12035-017-0622-3.

[13] H. Zhou, P. Zhu, J. Wang, H. Zhu, J. Ren, and Y. Chen, "Pathogenesis of cardiac ischemia reperfusion injury is associated with CK2-disturbed mitochondrial homeostasis via suppression of FUNDC1-related mitophagy," *Cell Death Differentiation*, vol. 25, pp. 1080–1093, Jun. 2018, doi: 10.1038/s41418-018-0086-7.

[14] L. Galluzzi, I. Vitale, and S. A. Aaronson, "Molecular mechanisms of cell death: Recommendations of the nomenclature committee on cell death 2018," *Cell Death Differentiation*, vol. 25, pp. 486–541, Mar. 2018, doi: 10.1038/s41418-017-0012-4.

[15] H. F. Zheng, *Foundation of Thermodynamics and Heat Transfer*. 1st ed. PR China: Science Press, 2016.

[16] T. Yang, Z. H. Fei, and X. M. Zhong, "Research progress of Caspase family and apoptosis," *Zhejiang Med. J.*, vol. 40, no. 18, pp. 2083–2091. 2018, doi: 10.12056/j.issn.1006-2785.2018.40.18.2017-950.

[17] S. L. Zhang, M. Y. Li, and Y. Y. Fan, "Advances in apoptotic cell clearance disorders and diseases," *Pharmaceutical Biotechnol.*, vol. 25, no. 2, pp. 86–90, 2018. [Online]. Available: http://kns.cnki.net/kcms/detail/detail.aspx?dbcode=CJFD&filename=YWSW201802017&dbname=CJFDLAST2018&uid=WEEvREcwSlJHSldRa1FhcEFLUmVhMFE2WDV3Y0g5dzkxK241SmI1WEN4bz0%3D%249A4hF_YAuvQ5obgVAqNKPCYcEjKensW4IQMovwHtwkF4VYPoHbKxJw, doi: 10.19526/j.cnki.1005-8915.20180217.

[18] K. F. Wu, *Principles of Cellular Social Ecology of Immunity*. PR China: Science Press, 2012.

[19] K. Wang, Y. Zhang, and S. B. Song, "Infrared image segmentation based on improved dimensional OTSU and genetic algorithm," *J. Syst. Simul.*, vol. 29, no. 6, pp. 1229–1236, 2017, doi: 10.16182/j.issn1004731x.joss.201706010.

[20] Z. J. Zhang, W. Ding, and L. Y. Xiao, "Extraction method of high temperature region in petrochemical thermal insulation pipeline based on threshold segmentation," *Comput. Era*, vol. 08, pp. 15–17, Aug. 2015. [Online]. Available: https://kns.cnki.net/KCMS/detail/detail.aspx?dbcode=CJFQ&dbname=CJFDLAST2015&filename=JSJS201508006&uid=WEEvREcwSlJHSldRa1FhcEFLUmVhMFE2WDV3ZjJtRFRIRWxoSitnbERBTT0=$9A4hF_YAuvQ5obgVAqNKPCYcEjKensW4IQMovwHtwkF4VYPoHbKxJw!!&v=MDIzMTJUM3FUcldNMUZyQ1VSN3FmWk9ab0ZpRGdXNzdCTHo3QmZiRzRIOVRNcDQ5RllvUjhlWDFMdXhZUzdEaDE=, doi: 10.16644/j.cnki.cn33-1094/tp.2015.08.006.

XIAO YU was born in 1985 in Linyi, China. He received the bachelor's degree from Qingdao University, in 2007, the master's degree from Qingdao University, in 2010, and the Ph.D. degree, in 2014.

He came to Tianjin Polytechnic University as a Teacher. In 2010, he entered the Beijing University of Science and Technology to study for the Ph.D. degree. He is currently an Associate Professor with the School of Electrical and Electronic Engineering, Tianjin University of Technology. He engaged in image processing, pattern recognition, and other fields. During the Ph.D. degree, he received a Ph.D. Scholarship and an Excellent Fund Project. He presided over the National Natural Science Foundation and the Tianjin Fund during his work. His research interests are in the fields of artificial immunity and image processing.

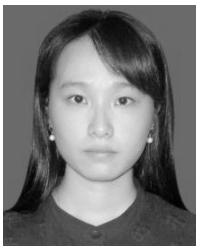

XI YE was born in Sichuan, China, in 1996. She received the bachelor's degree from the Tianjin University of Technology, in 2018, where she is currently pursuing the master's degree.

Since 2018, she has been learning about image processing and artificial immune theory, and combining them, and she has her own understanding of target extraction algorithms in infrared images.

QIANG GAO received the bachelor's degree in industrial automation from the Tianjin University of Technology, Tianjin, China, in 1990, and the master's degree in control theory and control engineering from Tianjin University, Tianjin, China, in 1999. He is currently a Professor with the School of Electrical and Electronic Engineering, Tianjin University of Technology. His research interests include brain–computer interface (BCI), industrial equipment fault diagnosis, and intelligent algorithms of quad-rotor UAV.